NASA Technical Memorandum 83062

NASA-TM-83062 19830011846

Precision Optical Angular Position Marker System for Rotating Machinery

John P. Barranger
Lewis Research Center
Cleveland, Ohio

February 1983

NASA

PRECISION OPTICAL ANGULAR POSITION MARKER SYSTEM

FOR ROTATING MACHINERY

John P. Barranger

National Aeronautics and Space Administration
Lewis Research Center
Cleveland, Ohio 44135

E-1533

SUMMARY

One or more markers of angular shaft position are often required as part of modern instrumentation for rotating machinery. The system described in this report consists of a light source, an optical cable, a machinery mounted lens assembly, a light detector, and a signal conditioner. Light reflected by targets on the rotor is converted to a digital output signal. The system is highly immune to vibration, can tolerate lens assembly temperatures up to 425° C, and has achieved an operational precision of 0.002 percent at a rotor rim velocity of 105 m/s.

INTRODUCTION

Advanced instrumentation for rotating machinery often requires precision markers of the angular shaft position while in operation. The High-Speed Laser Anemometer (ref. 1), for example, needs shaft position data within a precision of 0.01 percent. The Electronic Shaft Angle Encoder (refs. 1 and 2) generates this information from a precise once-per-revolution rotor marker.

Nonoptical methods using capacitance, magnetic, or eddy current sensors suffer from poor precision and temperature dependence. Moreover, they usually require a toothed rotor geometry and are subject to electrical interference.

This report describes a precision fiber optical angular position marker system for rotating machinery which overcomes some of the problems of the nonoptical methods. The system consists of a transmitter (light source), a bifurcated fiber optic cable, a machinery mounted lens assembly, and a receiver (light detector and signal conditioner). The light from the input fibers is imaged onto highly reflecting targets on the rotating component and reflected back to the output fibers. The resultant light pulses are converted to a digital output signal. A once-per-revolution marker is generated by a single target and angular position information may be provided from multiple targets.

The system is highly immume to extreme environments. The placement of the transmitter and receiver away from the machinery and the choice of solid state components minimize the damaging effects of machine vibration. Furthermore, the lens assembly can tolerate operating temperatures up to 425° C.

Performance tests were conducted on the system under laboratory and test cell operational environments. The system achieved a precision or repeatability of approximately 0.003 percent at a rim velocity of 139 m/s with a laboratory rotor and 0.002 percent at a rim velocity of 105 m/s under operational test conditions.

SYSTEM DESCRIPTION

System Block Diagram

Figure 1 is a block diagram of the angular position marker system. It consists of a transmitter (light source), a bifurcated fiber optic cable, a machinery mounted lens assembly, and a receiver (light detector and signal conditioner). Electrical power is supplied to the transmitter and receiver. Optical connectors of the SMA type couple the fiber optic cable to the transmitter, to the receiver, and to a common connector at the lens assembly.

Light from the transmitter enters the input fiber bundle and is carried to the common connector. The light exits the input fibers and is imaged onto the highly reflective target on the rotating component. As the rotor turns pulses of reflected light are generated and reimaged onto the output fibers at the common connector. The light is carried by the output fiber bundle to the receiver for detection and signal conditioning. The receiver output consists of transistor-transistor-logic (TTL) digital pulses representing the reflected light.

The transmitter, receiver, and fiber optic cable, all meeting NASA specifications, were supplied by a commercial source. The lenses were standard catalog items.

Transmitter and Receiver

The electronic components selected for this system are commonly found in fiber optical communications systems. They are all solid state and possess the high reliability usually associated with this application.

The circuit schematic of the transmitter is shown in figure 2. A dc voltage source supplies the required current to a near infrared (830 nanometers wavelength) light emitting diode (LED). The light output is rated at 10 mW minimum continuous power for a current of 85 mA. A control is provided to adjust the power output.

Figure 3 is a block diagram of the receiver. It consists of an integral silicon photodiode-amplifier, a level comparator, and a liner driver. Light pulses exiting the output fiber bundle are detected by a 1-mm diameter active region of the photodiode. The photodiode and amplifier combination has a 75-mV/μW sensitivity. Noise immunity is provided by biasing the level comparator at 100 mV. Thus a 1 1/3-μW minimum change in optical power is required to change the output of the level comparator and a 2 2/3-μW change is needed to provide a 3-dB power level margin over threshold. The line driver delivers TTL pulses representing the reflected light into a 50-ohm load.

In order to minimize the effects of temperature and vibration, the transmitter, receiver, and its associated power supply are contained in an environmental enclosure located a few meters away from the machinery. The choice of solid state components further reduces the chance of failure due to the nearby machine induced vibration.

Fiber Optic Cable and Lens Assembly

The bifurcated fiber optic cable is fabricated from two 5-meter long optical fiber bundles. Each leg consists of approximately 200 glass fibers with each fiber having a core diameter of 68 micrometers and a step index of refraction profile. The bundle diameter is 1.2 mm and, including the protective jacket, the outer diameter is 2.34 mm. The numerical aperture is

typically 0.66 and the optical power attenuation constant is a maximum of 750 dB/km. The fibers are combined side by side by the common end with a random arrangement of input and output fibers. The three ends of the cable are terminated by SMA type optical connectors.

The lens assembly together with the common end of the optical cable is shown in figure 4. The plane of the open end of the fibers as well as the plane of the target are positioned approximately at the focal plane of their respective lenses. Since similar surfaces face each other, the effective magnification is approximately unity. The low f-number (approximately f/0.75) of the convex side of the convex-aspheric lens allows a high throughput of optical power from input fibers to the target and back to the output fibers. Optimum coupling is achieved by fine adjusting the cable-to-lens spacing and/or the lens-to-target spacing for maximum signal output from the photodiode-amplifier. With cooling, the lens assembly can tolerate operating temperatures up to 425° C.

The target material may be selected from a number of highly specular reflecting metals. Gold has a very high reflectance but is soft and easily scratched. Aluminum is the most widely used material being highly reflective and resistant to minor abrasions. For oxidation and tarnish resistance at high temperature, and exceptional hardness and durability, rhodium is the best choice of available materials. The nontarget portion of the rotor has an optical black finish or coating.

The position and/or width of the targets may be encoded to furnish angular position information. The TTL output would in this case be sent to a decoder of pulse position and/or pulse width modulation for further signal processing. A single target, of course, generates a once-per-revolution marker.

System Power Analysis

An analysis of optical power losses is necessary to assess system performance. The critical points for optical power are shown in figure 5. The transmitter coupling loss is the loss between the LED output P1 and the input to the input fiber bundle P2. The principal sources of loss include the effects of mismatch in emitting area of the LED and the fiber bundle area, numerical aperture mismatch, gap separation, axial and angular misalignment, and Fresnel reflection at the interferences. The sources of receiver coupling loss are similar to those of the transmitter coupling loss. Details of typical coupling loss calculations can be found in reference 3.

The loss occurring at the lens assembly and target is represented by the difference between P3 and P4. The loss includes the effects of mismatch in fiber bundle area and the effective lens area, numerical aperture mismatch, component separation, axial and angular misalignment, Fresnel reflection at the interfaces and target material, and surface characteristics.

Table I represents the results of the power analysis of the system. The power levels are listed in terms of dBm and μW. The relative power level zero dBm refers to an optical power level of 1 mW or 1000 μW. Any other relative power level can therefore be found from the relation

$$\text{dBm} = 10 \log \frac{\text{power}(\mu\text{W})}{1000}$$

The numerical values in the table were determined by measurement and calculation. The dBm column was rounded off to the nearest units digit. The loss

assigned to the lens assembly and target was the maximum allowable loss calculated by subtracting the available power level P3 from the power level P4 required to achieve a 3-dB power level margin over threshold at the photodiode input P6. This loss is approximately 16 dB or equivalently a 40:1 power loss ratio.

LABORATORY AND OPERATIONAL PERFORMANCE

Performance tests were conducted on the system described in the above section under laboratory and test cell operational environments. A measurement of precision based on distance or spatial precision and a measurement of precision based on time or temporal precision were found for the system. A machined aluminum disk was the laboratory rotor and the coupling flange on a turbine component stand located in a test cell was used for the operational tests.

The laboratory tests were conducted on a 10-cm (4.0-in.) diameter aluminum rotor driven by an air turbine. The rim was sprayed with optical black paint except for a single 3 mm wide target strip which was left in the as-machined condition.

Figure 6 is a photograph of the oscilloscope display of the photodiode-amplifier output and the TTL output at the maximum test rim velocity of 139 m/s. Figure 7 is the same as figure 6 except that the time base has been expanded. The waveshapes were nearly identical for all velocities above 1 m/s. Below this minimum velocity the ac coupling distorts the waveforms. This is not a serious limitation since the normal operating speed of most rotors produce rim velocities well above this minimum.

From figure 7 it can be seen that the output of the photodiode-amplifier was 200 mV in amplitude or twice the threshold level of 100 mV. This represents a 3-dB power level margin over threshold. The figure also shows a threshold level difference between leading and trailing edges or hysteresis of approximately 40 mV. This provides additional noise immunity.

The spatial precision is dependent upon the uncertainty in surface distance as the photodiode-amplifier output passes through the level detector threshold. From figure 7 the sensitivity at threshold in terms of the rotor rim distance traveled is approximately 1 mm/200 mV. The uncertainty of the threshold of the level detector input is known to be less than 2 mV. Thus the uncertainty of the rotor rim distance is 0.01 mm and the spatial precision expressed as a percentage of the rotor circumference is found from

$$\text{Spatial precision (percent)} = \frac{0.01 \times 100}{\pi \times D(\text{mm})} \qquad (1)$$

where D is the diameter of the rotor. The spatial precision of the laboratory rotor was therefore approximately 0.003 percent.

The operational tests were conducted under a test cell environment on the 18-cm (7.0-in.) diameter external coupling flange of a turbine component test stand. An aluminum foil target was attached to the flange rim using a cyanoacrylate type of adhesive. Optical black paint covered the rest of the rim.

The output waveforms were essentially the same as figures 6 and 7 except for a slight loss in the amplitude of the photodiode-amplifier output. Thus the uncertainty of the rotor rim distance was nearly the same as that for the laboratory rotor. Using equation (1), the spatial precision during the operational tests was determined to be better than 0.002 percent.

The temporal precision is measured by observing the pulse-to-pulse jitter of the TTL output on an oscilloscope during testing. The uncertainty is one half of the total jitter observed and the temporal precision expressed as a percentage of the average period between pulses can be found from

$$\text{Temporal precision (percent)} = \frac{1/2 \times \text{total jitter (sec)} \times 100}{\text{Average period (sec)}}$$

During the measurement of temporal precision the observation time must be short compared to other time-based uncertainties such as the response time of speed control loops. Because of an inadequate air turbine speed controller the temporal precision for the laboratory test could not be determined. The temporal precision during operational turbine testing was measured however, resulting in a better than 0.002 percent precision up to the maximum test speed of 11 150 revolutions per minute. The temporal precision is numerically the same as the spatial precision, as would be expected for a system immune to vibration and electrical interference.

PERFORMANCE AT HIGH SURFACE VELOCITIES

The system performance for rotors with high target surface velocities was not determined experimentally. From the standpoint of the electronics alone, the principal limiting factor is the transient response of the receiver. An estimate of the maximum surface velocity can be made by extrapolation from rise time and velocity data gathered during the laboratory testing.

The rise time of the signal in figure 7 represents the time required for the light spot on the rotor to travel completely from the black painted region to the target region. The distance the surface moves during this time is independent of the velocity. Thus an inverse proportionality can be established that expresses the rise time and velocity at a given test condition such as that represented by figure 7 to that at any other condition such as at the minimum rise time and therefore the maximum velocity. The maximum target surface velocity can be calculated from

$$V_m = \frac{V \times T}{T_m}$$

where V_m is the maximum velocity, V and T are the velocity and rise time, respectively, at any test condition, and T_m is the minimum rise time. From figure 7 the signal rise time for a surface velocity of 139 m/s is approximately 5 μs. The minimum rise time of the receiver electronics was measured to be 1.4 μs. The maximum surface velocity is therefore approximately 500 m/s. It is estimated that a fourfold increase in this velocity can be achieved with improved receiver electronics.

CONCLUSIONS

A precision fiber optical angular position marker system for rotating machinery has been described. The system is highly immune to extreme environments of vibration and temperature and achieved a precision of 0.002 per- cent at a rim velocity of 105 m/s under operational conditions.

REFERENCES

1. Powell, J. A.; Strazisar, A. J.; and Seasholtz, R. G.: High-Speed Laser Anemometer System for Intrarotor Flow Mapping in Turbomachinery. NASA TP-1663, February 1982.
2. Technical Information Manual, Electronic Shaft Angle Encoder, Model 371, Real Time Systems, Inc., Mount Vernon, N. Y., September 1978.
3. Bowen, T.; and Gempe, H.: Impact of Coupling Efficiency on Fiber Optic System Performance. Electro-Optical Systems Design, August 1980, pp. 35-43.

TABLE I

System power analysis		
Point in the system	Output power level	
	dBm	μW
P1: LED output	+10	10 000
P2: Input to input fiber bundle	+2	1 500
P3: Output from input fiber bundle	-3	500
P4: Input to output fiber bundle	-19	12
P5: Output from output fiber bundle	-24	4
P6: Photodiode input	-26	2 2/3

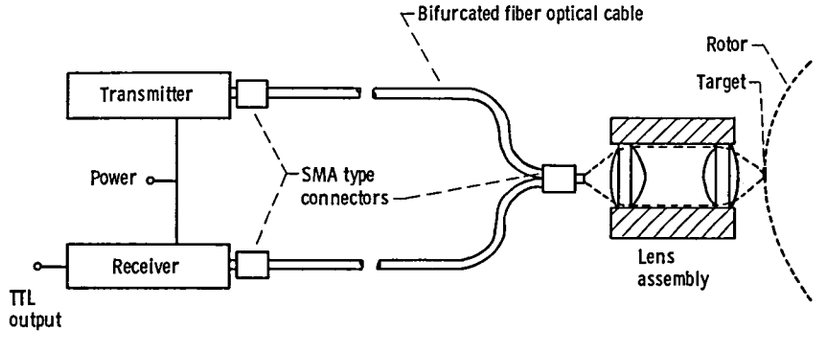

Figure 1. - Block diagram of angular position marker system.

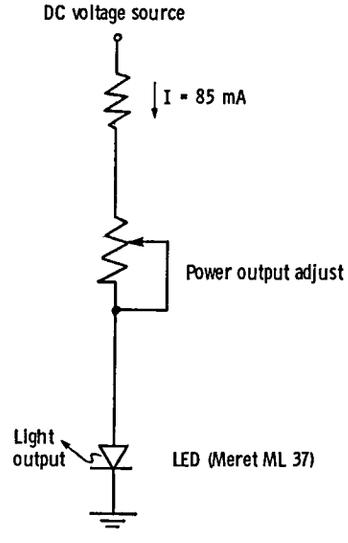

Figure 2. - Transmitter circuit schematic.

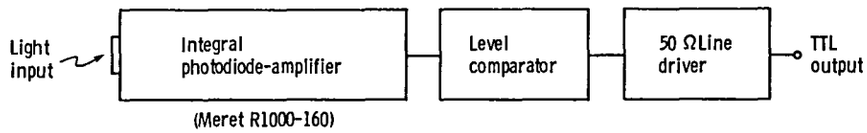

Figure 3. - Receiver block diagram.

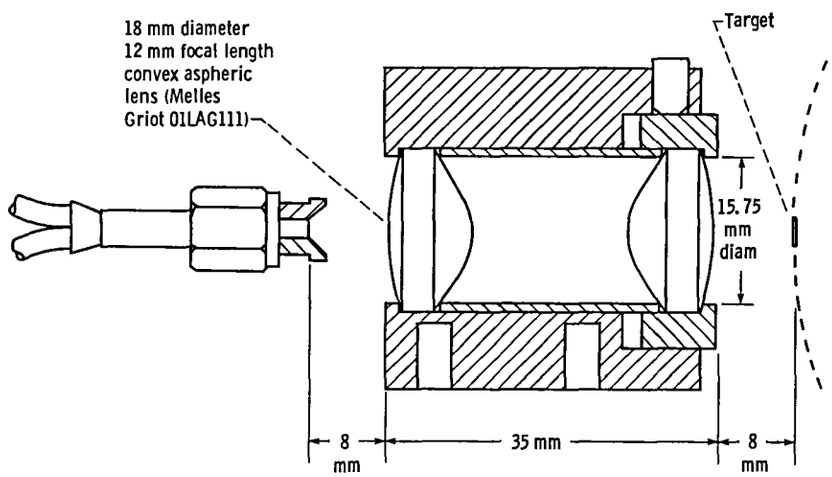

Figure 4. - Lens assembly.

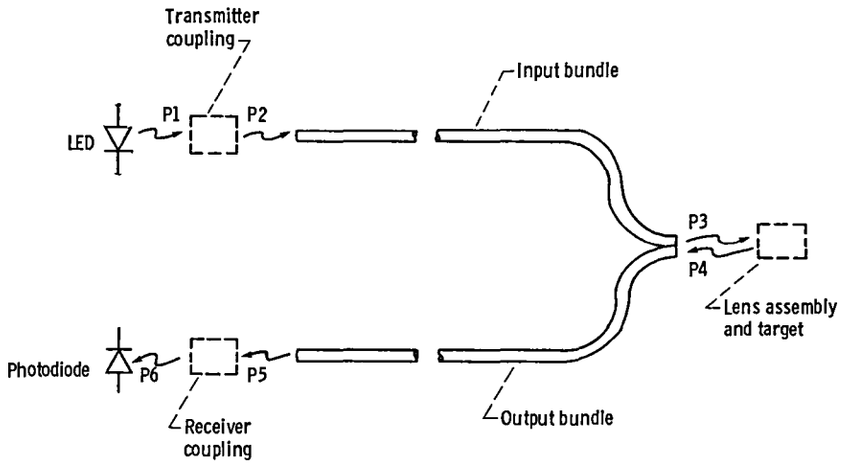

Figure 5. - System power points.

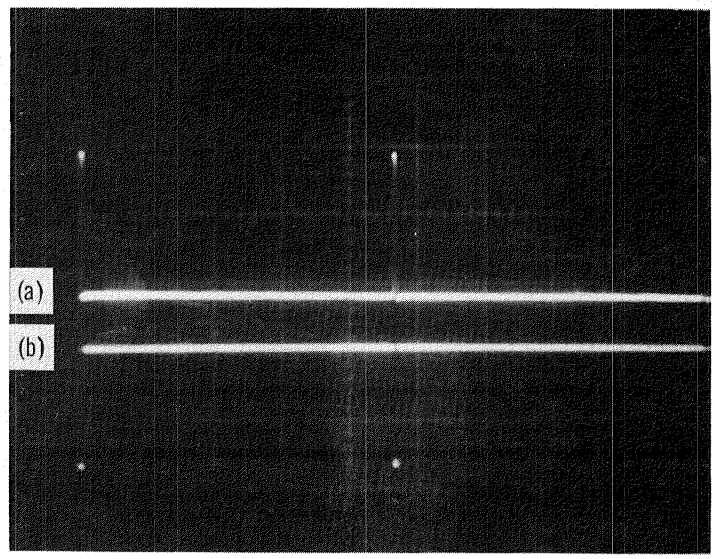

(a) Photodiode-amplifier output Vertical scale: 100 mV/div Horizontal scale: 0.5 msec/div.

(b) TTL Output Vertical scale: 2 V/div Horizontal scale: 0.5 msec/div.

Figure 6. - Oscilloscope display of pulses generated by the system for a laboratory rotor.

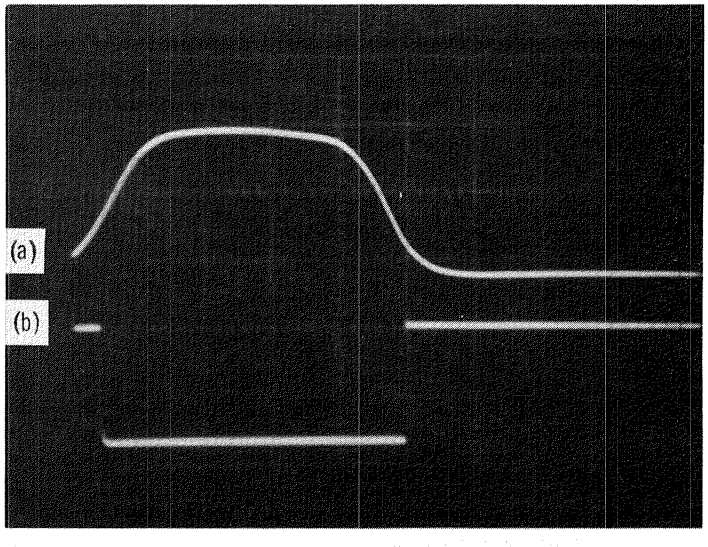

(a) Photodiode-amplifier output Vertical scale: 100 mV/div Horizontal scale: 5 μsec/div.

(b) TTL output Vertical scale: 2 V/div Horizontal scale: 5 μsec/div.

Figure 7. - Oscilloscope display of pulses generated by the system for a laboratory rotor (Time base expansion of Figure 6).

1. Report No.	2. Government Accession No.	3. Recipient's Catalog No.
NASA TM-83062		

4. Title and Subtitle	5. Report Date
PRECISION OPTICAL ANGULAR POSITION MARKER SYSTEM FOR ROTATING MACHINERY	February 1983
	6. Performing Organization Code 505-40-5A
7. Author(s)	8. Performing Organization Report No.
John P. Barranger	E-1533
	10. Work Unit No.
9. Performing Organization Name and Address	
National Aeronautics and Space Administration Lewis Research Center Cleveland, Ohio 44135	11. Contract or Grant No.
	13. Type of Report and Period Covered
12. Sponsoring Agency Name and Address	Technical Memorandum
National Aeronautics and Space Administration Washington, D.C. 20546	14. Sponsoring Agency Code

15. Supplementary Notes

16. Abstract

An optical system is described which generates one or more markers of the angular shaft position of rotating machinery. The system consists of a light source, an optical cable, a machinery mounted lens assembly, a light detector, and a signal conditioner. Light reflected by targets on the rotor is converted to a digital output signal. The system is highly immune to extreme environments of vibration and temperature and achieved a 0.002-percent precision under operational test conditions.

17. Key Words (Suggested by Author(s))	18. Distribution Statement
Turbomachinery Sensors and transducers Optics Nondestructive testing Solid state devices Amplifiers	Unclassified - unlimited STAR Category 37

19. Security Classif. (of this report)	20. Security Classif. (of this page)	21. No. of Pages	22. Price*
Unclassified	Unclassified		

* For sale by the National Technical Information Service, Springfield, Virginia 22161

End of Document